NASA TECHNICAL NOTE

NASA TN D-8333

NASA TN D-8333 c.1

ANALYTICAL STRUCTURAL EFFICIENCY STUDIES OF BORSIC/ALUMINUM COMPRESSION PANELS

Robert R. McWithey

Langley Research Center
Hampton, Va. 23665

NATIONAL AERONAUTICS AND SPACE ADMINISTRATION • WASHINGTON, D. C. • DECEMBER 1976

1. Report No. NASA TN D-8333	2. Government Accession No.
4. Title and Subtitle ANALYTICAL STRUCTURAL EFFICIENCY STUDIES OF BORSIC/ALUMINUM COMPRESSION PANELS	5. Report Date December 1976
	6. Performing Organization Code
7. Author(s) Robert R. McWithey	8. Performing Organization Report No. L-10689
9. Performing Organization Name and Address NASA Langley Research Center Hampton, VA 23665	10. Work Unit No. 743-01-01-03
	11. Contract or Grant No.
12. Sponsoring Agency Name and Address National Aeronautics and Space Administration Washington, DC 20546	13. Type of Report and Period Covered Technical Note
	14. Sponsoring Agency Code
15. Supplementary Notes	

16. Abstract

Analytically determined mass-strength curves, strain-strength curves, and dimensions are presented for structurally efficient hat-stiffened panels, corrugation-stiffened panels, hat-stiffened honeycomb-core sandwich panels, open-section corrugation panels, and honeycomb-core sandwich panels. The panels were assumed to be fabricated from either titanium, Borsic/aluminum, or a combination of these materials. Results indicate Borsic/aluminum panels and titanium panels reinforced with Borsic/aluminum are lighter and stiffer than comparably designed titanium panels. Furthermore, reinforced titanium panels have the same extensional stiffness as comparably designed Borsic/aluminum panels. For a given load, the structural efficiency of the hat-stiffened honeycomb-core sandwich panel is higher than the structural efficiency of the other stiffened panels.

17. Key Words (Suggested by Author(s)) Composites, Compression, Minimum mass, Optimization, Sandwich panels, Stiffened panels	18. Distribution Statement Unclassified - Unlimited Subject Category 39

19. Security Classif. (of this report)	20. Security Classif. (of this page)	21. No. of Pages	22. Price*
Unclassified	Unclassified	30	$3.75

* For sale by the National Technical Information Service, Springfield, Virginia 22161

ANALYTICAL STRUCTURAL EFFICIENCY STUDIES OF BORSIC/ALUMINUM COMPRESSION PANELS

Robert R. McWithey
Langley Research Center

SUMMARY

Analytically determined mass-strength curves, strain-strength curves, and dimensions are presented for structurally efficient hat-stiffened panels, corrugation-stiffened panels, hat-stiffened honeycomb-core sandwich panels, open-section corrugation panels, and honeycomb-core sandwich panels. The panels were assumed to be fabricated from either titanium, Borsic/aluminum, or a combination of these materials. Results indicate Borsic/aluminum panels and titanium panels reinforced with Borsic/aluminum are lighter and stiffer than comparably designed titanium panels. Furthermore, reinforced titanium panels have the same extensional stiffness as comparably designed Borsic/aluminum panels. For a given load, the structural efficiency of the hat-stiffened honeycomb-core sandwich panel is higher than the structural efficiency of the other stiffened panels.

INTRODUCTION

The structural properties of low-density advanced fibrous composite structural materials make their use attractive in aircraft compression panels. Furthermore, materials data for aluminum matrix composites indicate desirable material properties are still present at the moderately high steady-state temperatures experienced by supersonic flight vehicles. Thus, composite structures fabricated from materials such as boron/aluminum may offer both structural-mass reductions and increased structural stiffness when compared with similar titanium structures. These factors could have a significant impact on the viability of commercial supersonic vehicles.

In order to determine quantitatively the possible advantages offered by a metal-matrix-composite compression structure, an analytical and experimental program was undertaken to design, fabricate, and test metal-matrix-composite compression panels. Boron/aluminum that consists of silicon carbide coated boron filaments (commonly called Borsic filaments, the registered trademark name) encapsulated in a 6061 aluminum-alloy matrix was the composite material selected for the study. This material selection was based upon favorable material property data at elevated temperatures (see ref. 1), availability, status of development, and apparent resistance to material degradation when subjected to short-term thermal cycles typically experienced in brazing aluminum composites (see ref. 2).

The present paper presents preliminary analytical results from this program that provide a perspective on the relative mass and stiffness perform-

ance of the five titanium and Borsic/aluminum (hereinafter denoted as Bsc/Al) composite compression panel configurations shown in figure 1. Fabrication of Bsc/Al panels with these configurations is within the state-of-the-art using preconsolidated sheet material, unidirectional laminates (0° laminates) in the stiffeners, and conventional joining processes for attaching the skins and stiffeners (see ref. 2).

SYMBOLS

b	plate width or panel width
D	bending stiffness
d	stiffener height
E	Young's modulus
E_{11}	Young's modulus of unidirectional composite material in fiber direction
E_{22}	Young's modulus of unidirectional composite material transverse to fiber direction
G	shear modulus
G_{12}	shear modulus of unidirectional composite material relative to fiber direction
h	core height
L	panel length
m_{cr}	number of longitudinal half-wavelengths in buckle pattern
N_x	longitudinal load per unit width of panel
N_x/b	loading index for honeycomb-core sandwich panels
N_x/L	loading index for stiffened panels
t	plate thickness or skin thickness
w	mass per unit planform area of panel
w/b	mass parameter for honeycomb-core sandwich panels
w/L	mass parameter for stiffened panels
γ_{12}	shear strain relative to fiber direction
ϵ	extensional strain

ε_{11} extensional strain in fiber direction of unidirectional composite

ε_{22} extensional strain transverse to fiber direction in unidirectional composite

ν Poisson's ratio

ν_{12} principal Poisson's ratio of composite material

ρ density

σ stress

Subscripts:

comp compression

core honeycomb-core material

max maximum

n number of layers

s symmetric

Ti titanium

x longitudinal direction on panel

y transverse direction on panel

1,2,3,4 element number

FAILURE CRITERIA

In the present study the maximum load-carrying capability of the panel was assumed reached when the panel longitudinal strain reaches either a defined maximum allowable material strain in any panel element or a calculated strain for either local or overall panel buckling.

Elastic local buckling strains for the panels were analytically established in the present study from elastic laminate-plate theory and by assuming panel elements behave as simply supported, infinitely long flat plates. Material property data were taken from references 1, 3, and 4 and are presented in tables 1 to 3. Typical local buckling design curves resulting from this design approach are shown in figure 2(a) where longitudinal strain is plotted as a function of element b/t ratio.

The maximum strains indicated in the figure result from imposing the maximum-strain restrictions indicated in tables 1 and 2. These values of strain are assumed sufficient to restrict material and laminate behavior to

linear elastic regions of their corresponding stress-strain curves. For Bsc/Al laminates containing $\pm 45^{\circ}$ laminates, the $\gamma_{12,max} = 0.006$ restriction (table 2) limits the maximum longitudinal strain of this laminate to approximately 0.0047.

Although this design approach is valid for a wide range of closed-section stiffener configurations using isotropic and graphite-epoxy materials, its validity has not been established for use with Bsc/Al composites. Unfortunately, there are limited data on the compressive strength of boron/aluminum or Bsc/Al panels. A comparison between experimental compression strength data (from refs. 2 and 5) for unidirectional Bsc/Al plates and the local buckling design curve for unidirectional Bsc/Al used in the present analysis is shown in figure 2(b). The solid line in figure 2(b) denotes the design curve from the present analysis used for 0° Bsc/Al laminae that has a limiting stress value corresponding to a maximum permissible longitudinal strain of 0.0066 as indicated in table 2. The lower stress limit, indicated by the dashed line in figure 2(b), corresponds to a longitudinal strain of 0.0047. This limit would be imposed on the unidirectional plate elements when $\pm 45^{\circ}$ Bsc/Al laminae are present elsewhere in the panel cross section. The solid-circle symbols present ultimate compression failure data from reference 5 in which unidirectional boron/aluminum plates were supported in V-grooves during loading. These data, when compared with the design curve from the present analysis, indicate ultimate strengths less than the buckling strength over a wide range of b/t values. This comparison indicates that the test results of reference 5 may have been adversely affected by transverse compressive stress from the V-groove supports, and/or initial imperfections and transverse plasticity. Buckling test data (from ref. 2 and unpublished data from the authors of ref. 2) on unidirectional Bsc/Al hat-stiffened panels with no lateral displacement constraints are shown by the open-circle symbols in figure 2(b) and indicate buckling stresses as much as 30 percent higher than the ultimate failure stresses reported in reference 5. Although the reason for the discrepancy between the test results of references 2 and 5 is not thoroughly understood at the present time, the data from reference 2 suggest that the proposed failure criteria are reasonable for a preliminary design study.

ANALYSIS

Panel Optimization Procedure

An optimization procedure similar to the procedure presented in reference 6, which incorporates nonlinear mathematical programing techniques and uses panel mass as the performance function, was used to obtain dimensions of the configurations shown in figure 1 that result in minimum-mass configurations for specified longitudinal compression loads. During the optimization procedure for the longitudinally stiffened panel configurations, the panels are analyzed as a wide column. Thus, for these configurations general instability is characterized by Euler column buckling. Local instability is characterized by the buckling of the plate elements shown in sketch (a). Each plate element is assumed simply supported and infinitely long and may be

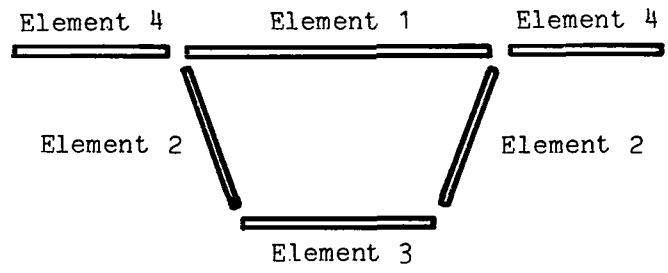

Sketch (a)

layered and orthotropic. In addition, the procedure maintains uniform longitudinal strains on the cross section.

Structurally efficient sandwich panels (configuration 5, fig. 1) with orthotropic face sheets were also obtained using this procedure. For this configuration, general instability of the panel was considered by treating the panel as a simply supported infinitely long flat plate. Equations developed in reference 7 were used to define structurally efficient sandwich panels having isotropic face sheets.

Constraints in the optimization process are: (a) the applied load must not be greater than the Euler buckling load for the column, (b) the loads in the individual plate elements must not be greater than their corresponding buckling loads, (c) the strains in the laminae must not be greater than maximum strains prescribed by the user, and (d) the dimensions of each lamina are within the limits prescribed by the user.

Transverse shear deformations, which may be significant for configurations incorporating honeycomb-core sandwich panels (configurations 3 and 5, fig. 1), are not considered in the panel optimization procedure described previously. The effects of transverse shear deformation on the load-carrying capability of designs produced by the optimization procedure for configurations 3 and 5 were determined using the equations presented in reference 8.

Buclasp 2 Program

Buckling modes that are more complex than the modes incorporated in the optimization procedure may allow panel designs, which were produced by the optimization procedure, to become unstable at loads less than their design load. In order to verify the load-carrying capability of the designs produced by the optimization procedure, several designs were analyzed using the Buclasp 2 computer program. This program, which is described in detail in references 9 and 10, performs an exact linear elastic buckling analysis on structures with constant cross section that may be idealized by an assembly of flat and curved plate elements and beam elements. Edges of the structure normal to the longitudinal axis are simply supported, and edges parallel to the longitudinal axis may be constrained as desired by the user. Buckling modes are determined from the total stiffness matrix of the structure and

thus are not limited to the buckling modes prescribed in the optimization procedure.

In the present study cross sections obtained from the optimization procedure were used to form a comparable Buclasp 2 model for a multibay panel with either free-free or symmetrical edge restraints. The model was then analyzed (usually for an aspect ratio of 2) to determine the lowest buckling load and corresponding mode shape. These results were compared with results from the optimization procedure.

RESULTS AND DISCUSSION

The principal results from the present analyses are the relationships that were developed between panel mass, longitudinal strain, and panel strength for structurally efficient compression panels of the types shown in figure 1. These relationships are shown in figures 3 to 7 and are discussed in the following sections of this report. Structurally efficient panel designs were obtained for titanium panels, Bsc/Al panels, and panels containing both titanium and Bsc/Al. Titanium honeycomb-core material was incorporated in all designs containing a honeycomb core. Because of interest in applications for supersonic aircraft, results from the titanium-panel analyses are used as a basis for comparing the mass and strain of the other panel designs of each configuration. In addition, a mass comparison between the panel configurations shown in figure 1 is presented in figure 8, and the effects of minimum gage constraints on the mass of structurally efficient hat-stiffened panels are briefly discussed with the use of figure 9. Dimensions of structurally efficient designs are presented in table 4 and in figure 7(c).

Hat-Stiffened Panels (Configuration 1)

Five types of hat-stiffened panels were examined and are shown in figure 3(a). The effect of stacking sequence and angle plies on the mass and stiffness of the all-composite configurations (configurations 1b to 1d) was studied to indicate optimum stacking and ply configurations. Configuration 1e is included to determine changes in structural efficiency when titanium hat stiffeners are incorporated in Bsc/Al panels.

Mass-strength curves for these configurations (see fig. 3(b)) indicate buckling constraints govern panel mass up to a load index value of approximately $N_x/L \approx 5.5$ MN/m^2 (800 lbf/in^2). Beyond this value maximum strain constraints generally govern panel mass. The curves also indicate that composite panels offer a 50-percent mass reduction over corresponding titanium panels in the buckling constrained region. Since configurations 1c and 1d give the same results, the angle-ply laminae and stacking sequence of angle-ply laminae have no significant effect on composite panel mass. A brief discussion of the effect of angle plies and stacking sequence on panel mass is presented in appendix A. Structurally efficient panels with reinforced titanium hats and Bsc/Al skins (configuration 1e) offer approximately a 30-percent mass reduction over corresponding titanium panels.

Optimum panel designs for configuration 1c at load index values of 1.38 MN/m^2 (200 lbf/in^2) and 4.14 MN/m^2 (600 lbf/in^2) and a length of 178 cm (70 in.) were analyzed using Buclasp 2. The minimum buckling load index values derived from the Buclasp 2 analysis are denoted in figure 3(b) by the open-circle symbols and are identical with the values obtained from the optimization procedure. The Buclasp 2 analysis for both free and symmetric-edge boundary conditions indicates the panel buckling mode to be similar to the first Euler column mode. No significant distortions were apparent in the stiffener elements or the skin. The panel optimization procedure also indicated the panel buckling mode was the first Euler column mode. Thus, for this design, the agreement between the results of the Buclasp 2 analysis and the optimization analysis supports the validity of the optimization procedure.

Longitudinal compressive strains of optimum designs are shown in figure 3(c) as a function of the load index N_x/L. The limiting strain value shown for the titanium panel is the maximum longitudinal compressive strain of the material as given in table 1. The limiting longitudinal strain value for the panels containing $\pm 45^\circ$ laminae was determined by the shear strain in the angle-ply laminae ($\gamma_{12,max} = 0.006$ in table 2).

Several interesting results may be concluded from the figure. First, the Bsc/Al designs are approximately $1\frac{1}{2}$ times more stiff than the optimum titanium designs. This result differs from the results, presented in reference 11, of a similar comparison between optimum graphite-epoxy panels and aluminum panels. Reference 11 indicates optimum graphite-epoxy composite panels may possess less inplane stiffness than optimum aluminum panels. Thus, replacement of optimum titanium panels with optimum Bsc/Al compression panels will increase the inplane stiffness of the structure. In addition, optimum panel designs having a Bsc/Al skin and reinforced titanium hat stiffeners have the same stiffness as optimum Bsc/Al designs. Thus, high inplane stiffness may be achieved without the complexity of fabricating panels entirely from Bsc/Al composite material.

The open-circle symbols in figure 3(c) indicate design points from the Buclasp 2 analyses. Buclasp 2 results give buckling strains equal to the strains from the optimization analysis.

Corrugation-Stiffened Panels (Configuration 2)

Three types of corrugation-stiffened panels were examined and are shown in figure 4(a). These configurations differ from the hat-stiffened panel configurations because the corrugated stiffeners, which may be fabricated as one continuous stiffener, provide additional skin material between stiffeners that allows an increase in stiffener spacing.

Comparison of mass-strength results (fig. 4(b)) and strain-strength results (fig. 4(c)) for configuration 2 indicates results similar to those for configuration 1. Furthermore, comparison of panel masses between designs

for configurations 1 and 2 indicates corrugation-stiffened panel designs are slightly heavier than comparable hat-stiffened panels.

The mass-strength curve shown in figure 4(b) for graphite-epoxy panels of similar configuration was taken from reference 6. The curves indicate graphite-epoxy panels are approximately 30 percent lighter than the Bsc/Al panels.

Hat-Stiffened Honeycomb-Core Sandwich Panels (Configuration 3)

Three types of hat-stiffened honeycomb-core sandwich panels were examined and are shown in figure 5(a). The density of the titanium honeycomb core was 160 kg/m^3 (10 lbm/ft^3).

Mass-strength curves for these configurations (see fig. 5(b)) indicate buckling constraints govern panel mass up to a range of load index values from $N_x/L = 1.38$ MN/m^2 (200 lbf/in^2) to $N_x/L = 2.07$ MN/m^2 (300 lbf/in^2). The curves also indicate composite panels offer a 40-percent mass reduction over corresponding titanium panels for the entire load range shown.

Mass comparisons between hat-stiffened sandwich panels (configuration 3) and the hat-stiffened panels of configuration 1 indicate configuration 3 titanium panels are approximately 40 percent lighter than those of configuration 1 for configuration 3 designs influenced only by buckling criteria. Similarly, configuration 3 composite panels are approximately 30 percent lighter than those of configuration 1. After maximum strain criteria become effective in configuration 3 designs, the difference in mass between configuration 1 and configuration 3 designs decreases and the cross sections of configuration 1 and configuration 3 designs become similar.

Compressive strain-strength curves for the stiffened sandwich designs are shown in figure 5(c). The composite panel designs are approximately $1\frac{1}{2}$ times more stiff than comparable titanium designs. Comparison between the strains for configuration 1 (fig. 3(c)) and configuration 3 indicate configuration 1 designs are 1.7 times more stiff than configuration 3 designs for low values of the load index.

The open-circle symbols in figures 5(b) and 5(c) represent results from a Buclasp 2 analysis of the design produced by the optimization procedure for a load index of 1.38 MN/m^2 (200 lbf/m^2) and a panel length of 177.8 cm (70 in.). As indicated, the Buclasp 2 analysis, which incorporated symmetric boundary conditions along the panel edges, gives excellent agreement with the results from the optimization procedure. The buckling mode shape from the Buclasp analysis was the first Euler column mode. This mode agrees with the buckling mode from the optimization procedure for this design.

Analyses to determine the effects of transverse shear deformations on the sandwich-skin buckling loads produced by the optimization procedure were

made using equations presented in reference 8. The results indicate that sandwich-skin buckling loads are reduced less than 5 percent.

Open-Section Corrugation Panels (Configuration 4)

Three types of open-section corrugation panels were examined and are shown in figure 6(a). No angle-ply laminae were incorporated in these configurations because of difficulties expected in attaining small bend radii during fabrication with angle-ply laminae.

Mass-strength curves for these configurations (see fig. 6(b)) indicate buckling criteria govern panel mass up to a load index of approximately $N_x/L = 4.83$ MN/m^2 (700 lbf/in^2) for the titanium designs and $N_x/L = 6.89$ MN/m^2 (1000 lbf/in^2) for the composite designs. The curves also indicate the composite panel designs offer a 50-percent mass reduction over corresponding titanium panels. In addition, configuration 4a and configuration 4b designs offer a 15-percent mass reduction over comparable configuration 1 designs. The reinforced titanium designs (configuration 4c) are approximately 20 percent lighter than the titanium designs.

Compressive strain-strength curves for configurations 4a and 4b are shown in figure 6(c). The composite panel designs are approximately $1\frac{1}{2}$ times more stiff than comparable titanium designs. Comparison between the strains for configuration 1 and configuration 4 indicate configuration 1 designs are slightly more stiff than configuration 4 designs.

The open-circle symbols in figures 6(b) and 6(c) represent results from Buclasp 2 analyses of the designs produced by the optimization procedure for load indexes of 1.38 MN/m^2 (200 lbf/m^2) and 6.89 MN/m^2 (1000 lbf/m^2) and a panel length of 177.8 cm (70 in.). The Buclasp 2 analyses, which incorporated symmetric boundary conditions along the panel edges, give excellent agreement with the results from the optimization procedure except that the Buclasp 2 analysis predicts a slightly lower buckling strain than the optimization procedure at the higher value of load index. The buckling modes from the Buclasp 2 analyses are local buckling modes in which all elements behave as simply supported plates. This result is consistent with the constraints and results from the optimization procedure.

Honeycomb-Core Sandwich Panels (Configuration 5)

Three types of honeycomb-core sandwich panels were examined and are shown in figure 7(a). These configurations were selected to compare the structural efficiency of sandwich panels and stiffened panels. The panels shown in figure 7(a) were analyzed as infinitely long, simply supported panels. This analysis differs from the stiffened-panel analysis in which the wide-column analogy was applicable. Details of the configuration 5 analysis are presented in appendix B.

Figure 7(b) presents the mass-strength results for the configurations shown in figure 7(a). Using configuration 5b results as a basis for comparison, the less dense core designs (configuration 5a) result in a 28-percent mass decrease at the lower load index values and a 12-percent mass decrease at a load index value of approximately 2.5 MN/m^2 (360 lbf/in^2). Similarly, the configuration with composite face sheets results in a 28-percent mass decrease at the lower load index values and a 36-percent mass decrease at a load index value of 2.5 MN/m^2 (360 lbf/in^2). Figure 7(b) also indicates that the change in panel mass that results from consideration of the core shear stiffness is negligible.

The panel designs associated with figure 7(b) are constrained by maximum strain criteria. Thus, the compressive strain for configurations 5a and 5b is 0.0078, and the compressive strain for configuration 5c is approximately 0.0047.

Panel dimensions for configuration 5 designs may be obtained from figure 7(c) as a function of load index. Since panel designs are governed by maximum strain constraints, cover-sheet thickness is a linear function of load index. The relations between core height and load index for various values of core shear stiffness indicate only modest increases in core height are required when core shear stiffness is considered in the design process.

Figure 8 presents optimum panel masses for configurations 1 through 5 for a load of N_x = 1.75 MN/m (10 000 lbf/in.) and a panel width of 88.9 cm (35 in.) as a function of panel aspect ratio. The optimum panel masses are valid for aspect ratios greater than 1 (see discussion in appendix B). The honeycomb-core density for configurations 3 and 5 is 160 kg/m^3 (10 lbm/ft^3). This figure indicates that titanium hat-stiffened honeycomb-core sandwich panels are mass competitive with configuration 5 panels for hat-stiffened panel lengths less than 145 cm (57 in.). Similar results are shown for optimum composite panels. Figure 8 indicates that optimum composite panels for configurations 1, 3, and 4 are mass competitive with configuration 5 panels for configurations 1, 3, and 4 panel lengths less than 88.9 cm (35 in.), 198 cm (78 in.), and 137 cm (54 in.), respectively. Comparison of extensional strains for the designs where configurations have the same mass indicates all stiffened panel designs are more stiff than the unstiffened sandwich panel designs.

The wide-column assumption for the stiffened designs is a conservative assumption, and actual buckling loads would be greater for these designs with simply supported sides. Thus, the panel masses shown in figure 8 for stiffened panels would be reduced if simply supported boundary conditions were used in an optimization procedure for full-sized panels.

Comparison of masses between the optimum unstiffened sandwich titanium panel (configuration 5b) and the unstiffened sandwich composite panel (configuration 5c) indicates that the composite panel design offers a 35-percent mass reduction over the lengths investigated.

Minimum Gage Constraints

Minimum gage constraints were not considered in the foregoing discussions. The effect of minimum gage constraints on panel mass for configurations 1 to 4 is a function of panel length (minimum gage constraint effects on panel mass decrease with increasing panel length), loading index, and panel material. For the mass-strength curves presented in figures 3, 4, 5, and 6, panel lengths and the minimum load-index value were selected so that minimum gage constraints could be neglected. Figure 9 shows the results of analyses on configurations 1a and 1c for values of $N_x/L > 0.07$ MN/m^2 (10 lbf/in^2) to determine the effects of minimum gage constraints. Minimum gages used in the analysis are shown in the figure. (The minimum gage for the unidirectional material in the skin of configuration 1c was zero.) For the load range shown, the results indicate that the minimum gage constraints imposed on the titanium panels had no effect on panel mass for the 177.8-cm (70-in.) length panels and affect the mass of the 63.5-cm (25-in.) panels for load index values below $N_x/L = 276$ kN/m^2 (40 lbf/in^2). (The tick marks indicate the approximate maximum value of load index for which minimum gage constraints affect panel mass.)

Results for the composite panel indicate minimum gage constraints have a more pronounced effect on the mass of these panels. This result is largely caused by the angle-ply minimum gage constraint. The dashed line indicates the mass of composite panel designs without the minimum gage constraints.

Summary of Structural Efficiency Studies

Figure 10 presents a summary of the buckling and maximum strain constrained mass-strength curves for a range of load indices expected in aircraft lifting surfaces and for the four titanium and Bsc/Al panel configurations analyzed as wide columns. It may be seen that all minimum-mass composite panels are lighter than minimum-mass titanium panels. For a given material, buckling critical panels listed in order of increasing mass are:

(a) Hat-stiffened honeycomb-core sandwich panels

(b) Open-section corrugation panels

(c) Hat-stiffened panels

(d) Corrugation-stiffened panels

Panel dimensions of several configurations are given in table 4 for various values of load index and panel length. Element widths and element numbers are defined in the sketch presented in table 4. The relative position of a lamina within an element is defined in table 4 by the numbers in parentheses (for example, (1,1)) where the first number, 1, locates the position of the lamina at the midplane of the laminate and the second number, 1, defines the element number, 1, as shown in the table 4 sketch. Correlations between the lamina thickness and ply angle within a laminate may be made using table 4 and the configuration cross sections shown in figures 3 to 6.

The results shown in table 4 indicate that Euler column buckling is a governing constraint in all optimum designs except the highly loaded designs in which maximum strain constraints govern panel design. This result is in agreement with the Buclasp 2 buckling-mode predictions for configurations 1 and 3. In the configuration 4 designs shown in table 4, both Euler column buckling and local buckling constrain panel design. The Buclasp 2 analyses for this configuration indicated the local buckling mode to be the lowest buckling mode.

Another result indicated in table 4 is that, for configuration 1c designs for panel lengths of 177.8 cm (70 in.) and 63.5 cm (25 in.), no 0° Bsc/Al laminae are required in the skin of the shorter panel. In addition, the configuration 3b designs indicate that increasing the panel compression load results in a decrease of the honeycomb-core thickness (see laminae (1,1) and (1,4) in table 4).

CONCLUDING REMARKS

The present study has provided a perspective on the relative mass and stiffness performance of five compression panel configurations fabricated from titanium, Borsic/aluminum, or a combination of these materials. Agreement between elastic buckling theory and experimental results from reference 2 for unidirectional Borsic/aluminum hat-stiffened panels indicate elastic buckling theory may be used in preliminary design of Borsic/aluminum compression panels. Thus, elastic buckling design criteria and plate laminate theory were used to determine optimum structural mass and stiffness in the present study. The results are presented in the form of mass-strength curves and strain-strength curves.

The following specific conclusions may be made from the study:

1. For the structurally efficient compression-panel configurations and compression-load ranges studied:

(a) Composite panels will have 35 percent to 50 percent less mass than efficient titanium panels carrying the same load.

(b) Inplane longitudinal stiffness of Borsic/aluminum composite panels is from 25 to 45 percent higher than the stiffness of titanium panels.

(c) Borsic/aluminum composite reinforced titanium panels will possess 20 to 35 percent less mass than titanium panels.

(d) Inplane stiffness of reinforced titanium panels is approximately the same as the stiffness of composite panels.

2. For a given load level and panel width, the mass of the longitudinally stiffened panels increases with increasing panel length. Thus, for sufficiently long panels, the honeycomb-core sandwich panel becomes the most efficient structural configuration of the configurations under investigation.

3. Panel mass is nearly independent of orientation of angle-ply layers in buckling constrained designs.

4. Effects of minimum gage constraints are greater in composite designs than in titanium designs.

5. A refined buckling analysis indicates the buckling-mode assumptions used in the optimization procedure are adequate for preliminary design.

6. For the stiffened configurations studied, the hat-stiffened honeycomb-core sandwich panels showed the highest structural efficiency.

Langley Research Center
National Aeronautics and Space Administration
Hampton, VA 23665
October 28, 1976

APPENDIX A

EFFECT OF ANGLE PLIES AND STACKING SEQUENCE OF COMPOSITE SKIN ON MASS OF BORSIC/ALUMINUM COMPRESSION PANELS

The optimization procedure was used to study the effect of angle-ply laminates and stacking sequence on configurations similar to configurations 1c and 1d. In this study, the skin is formed from 0° ply and angle-ply laminae. The angle-ply laminae were varied in 15° increments from 0° (unidirectional laminae) to 90° laminae. The results of this study indicate no perceptible change in panel mass as a function of ply angle. A slight decrease in mass may be achieved by using the angle plies on the exterior surface of the skin. Since panel mass is not a function of ply angle, $\pm 45^{\circ}$ angle-ply laminae were chosen for the main study because of their shear-carrying capability. (No shear loads were considered in the present study, however.)

APPENDIX B

ANALYSIS OF HONEYCOMB-CORE SANDWICH PANELS (CONFIGURATION 5)

The mass parameter w/L and load index N_x/L used in mass comparisons for configurations 1 through 4 are inappropriate for honeycomb-core sandwich panels. The previous configurations generally exhibit wide column behavior and derive minimal stiffness from simply supported edge conditions. This behavior can be expected when the transverse bending stiffness of the panel is small in comparison with the longitudinal bending stiffness. Furthermore, classical theory for simply supported orthotropic panels (ref. 12) indicates the panel buckling load is essentially independent of panel length for aspect ratios greater than $\sqrt[4]{D_x/D_y}$. For honeycomb-core panels with Bsc/Al face sheets comprised of $\pm 45^\circ$ and 0° laminae, $1 \leq \sqrt[4]{D_x/D_y} \leq 1.12$. Thus, mass-strength curves for configurations 5a through 5c are plotted in terms of the mass parameter w/b and load index N_x/b as shown in figure 7, and are valid for aspect ratios greater than approximately 1.

The mass-strength curves shown in figure 7 for titanium panels are derived using buckling equations that include the effect of transverse shear deformation as presented in reference 7 and the maximum strain constraint. In the analysis, the maximum strain constraint determines the cover-sheet thickness as a function of load and the buckling equation determines the core height required to maintain stability. The maximum strain constraint governs titanium panel design for load index values greater than 0.4 MN/m^2 (60 lbf/in^2).

The mass-strength curve shown in figure 7 for Bsc/Al panels (configuration 5c) was obtained using the optimization procedure. As with the titanium configuration, the cover-sheet thickness was determined by maximum strain constraints and the core height was determined by stability constraints.

REFERENCES

1. Kreider, Kenneth G., ed.: Metallic Matrix Composites. Academic Press, Inc., c.1974.

2. Royster, Dick M.; Wiant, H. Ross; and Bales, Thomas T.: Joining and Fabrication of Metal-Matrix Composite Materials. NASA TM X-3282, 1975.

3. Metallic Materials and Elements for Flight Vehicles Structures. MIL-HDBK-5, U.S. Dep. Def., Aug. 1962. (Supersedes MIL-HDBK-5, 1961.)

4. RohrBond™ - Titanium Honeycomb Structures. RHR-73-150, Rohr Ind., Inc., [1973].

5. Spier, E. E.: Crippling Analysis of Unidirectional Boron/Aluminum Composites in Compression Structures. Proceedings of the Conference on Fibrous Composites in Flight Vehicle Design, AFFDL-TR-72-130, U.S. Air Force, Sept. 1972, pp. 1151-1164. (Available from DDC as AD 907 942L.)

6. Agarwal, Banarsi; and Davis, Randall C.: Minimum-Weight Designs for Hat-Stiffened Composite Panels Under Uniaxial Compression. NASA TN D-7779, 1974.

7. Stein, Manual; and Mayers, J.: Compressive Buckling of Simply Supported Curved Plates and Cylinders of Sandwich Construction. NACA TN 2601, 1952.

8. Peterson, James P.: Plastic Buckling of Plates and Shells Under Biaxial Loading. NASA TN D-4706, 1968.

9. Viswanathan, A. V.; and Tamekuni, M.: Elastic Buckling Analysis for Composite Stiffened Panels and Other Structures Subjected to Biaxial Inplane Loads. NASA CR-2216, 1973.

10. Tripp, L. L.; Tamekuni, M.; and Viswanathan, A. V.: User's Manual - BUCLASP 2: A Computer Program for Instability Analysis of Biaxially Loaded Composite Stiffened Panels and Other Structures. NASA CR-112226, 1973.

11. Williams, Jerry G.; and Mikulas, Martin M., Jr.: Analytical and Experimental Study of Structurally Efficient Composite Hat-Stiffened Panels Loaded in Axial Compression. AIAA Paper No. 75-754, May 1975.

12. Lekhnitskii, S. G. (S. W. Tsai and T. Cheron, transl.): Anisotropic Plates. Gordon Breach Sci. Publ., Inc., c.1968.

TABLE 1.- TITANIUM MATERIAL PROPERTY DATA (REF. 3)

$E = 110\ GN/m^2\ (16.0 \times 10^6\ psi)$

$G = 43\ GN/m^2\ (6.2 \times 10^6\ psi)$

$\nu = 0.33$

$\epsilon_{max,comp} = -0.0078$

$\rho = 4400\ kg/m^3\ (0.16\ lbm/in^3)$

TABLE 2.- UNIDIRECTIONAL BORSIC/ALUMINUM MATERIAL PROPERTY DATA FOR 45-PERCENT FIBER VOLUME FRACTION (REF. 1)

$E_{11} = 207\ GN/m^2\ (30 \times 10^6\ psi)$

$E_{22} = 131\ GN/m^2\ (19 \times 10^6\ psi)$

$G_{12} = 57\ GN/m^2\ (8.3 \times 10^6\ psi)$

$\nu_{12} = 0.26$

$(\epsilon_{11,max})_{comp} = -0.0066$ (imposed in present analysis)

$\gamma_{12,max} = 0.006$ (imposed in present analysis)

$\rho = 2700\ kg/m^3\ (0.098\ lbm/in^3)$

TABLE 3.- TITANIUM HONEYCOMB PROPERTY DATA (REF. 4)

$$\begin{bmatrix} \rho = 80\ kg/m^3\ (5\ lbm/ft^3) \\ G = 380\ MN/m^2\ (55\ ksi) \end{bmatrix}$$

$$\begin{bmatrix} \rho = 160\ kg/m^3\ (10\ lbm/ft^3) \\ G = 760\ MN/m^2\ (110\ ksi) \end{bmatrix}$$

TABLE 4.- DIMENSIONS OF SELECTED MINIMUM-MASS PANELS

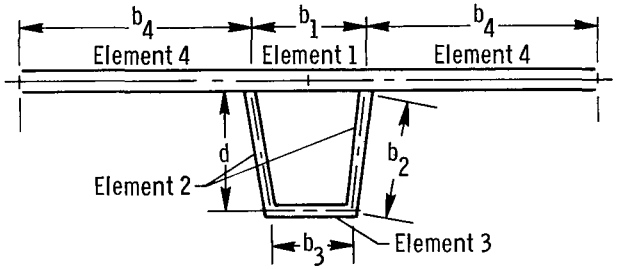

(a) SI Units

Configuration	N_x/L_1, MN/m^2	w/L, kg/m^3	$\varepsilon_x \times 10^3$	b_1, cm	b_2, cm	b_3, cm	b_4, cm	d, cm	L, cm	Lamina thickness, cm, for (lamina no., element no.) -									Elements at max. strain	Is column at Euler load?	Elements at local buckling
										(1,1)	(2,1)	(3,1)	(1,2)	(1,3)	(2,3)	(1,4)	(2,4)	(3,4)			
1a	1.38	15.5	3.56	7.63	8.01	7.89	3.81	8.01	177.8	0.236	-----	-----	0.248	0.248	-----	0.236	-----	-----	---	Yes	1,2,4
1b	1.38	7.65	2.36	6.55	6.41	6.36	3.28	6.41	177.8	.199	-----	-----	.195	.229	-----	.199	-----	-----	---	Yes	1,2,4
1c	1.38	7.73	2.63	2.76	2.45	2.37	1.38	2.44	63.5	*.071	0.0	-----	.079	.092	-----	*.071	0.0	-----	---	Yes	1,2,4
1c	1.38	7.80	2.41	7.30	6.36	5.82	3.65	6.31	177.8	*.071	*.071	-----	*.196	*.320	-----	*.071	*.071	-----	---	Yes	1,2,4
1c	6.89	19.4	4.73	7.27	10.2	6.78	3.68	10.1	177.8	*.071	*.164	-----	.438	.574	-----	*.071	.164	-----	1,4	No	2
1e	1.38	10.6	2.15	3.57	5.55	1.54	5.67	5.46	177.8	*.071	.123	-----	.133	.133	0.937	*.071	.123	-----	---	Yes	2,4
2a	1.38	17.2	3.22	4.26	5.06	3.11	5.06	5.03	127.0	.149	-----	-----	.149	.627	-----	.297	-----	-----	---	Yes	2,4
2b	1.38	8.32	2.17	4.21	4.21	4.39	3.49	4.21	127.0	.123	-----	-----	.123	.248	-----	.246	-----	-----	---	Yes	1,2
2c	1.38	14.0	2.00	2.82	3.71	1.43	5.39	3.64	127.0	.086	-----	-----	.086	.086	.889	.158	.086	-----	---	Yes	1,2
3a	1.38	9.81	6.09	13.2	10.8	10.4	18.1	10.7	177.8	.803	.041	-----	.437	.437	-----	.803	.041	-----	---	Yes	2,4
3b	1.38	5.41	3.84	10.5	8.75	8.63	13.2	8.70	177.8	.445	*.036	0.0	.339	.403	-----	.445	*.036	0.0	---	Yes	2,4
3b	6.89	19.6	4.71	10.9	12.9	10.6	5.79	12.9	177.8	.145	*.036	.082	.583	.786	-----	.145	*.036	.082	1,4	No	4
3c	1.38	7.26	4.64	8.38	8.53	4.88	19.0	8.34	177.8	.753	*.036	.012	.301	.301	.494	.753	*.036	.012	1,4	Yes	2,4
4a	1.38	12.8	4.32	15.1	9.26	10.3	5.14	8.95	177.8	-----	-----	-----	.315	.350	-----	.350	-----	-----	---	Yes	2,3,4
4b	1.38	6.48	2.79	12.0	6.93	9.49	4.74	6.81	177.8	-----	-----	-----	.229	.314	-----	.314	-----	-----	---	Yes	2,3,4

*This dimension was part of optimization-procedure input data.

TABLE 4.- Concluded

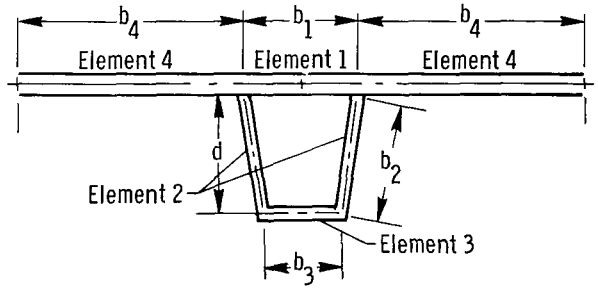

(b) U.S. Customary Units

Configuration	N_x/L, lbf/in^2	$w/L \times 10^4$, lbm/in^3	$\epsilon_x \times 10^3$	b_1, in.	b_2, in.	b_3, in.	b_4, in.	d, in.	L, in.	Lamina thickness, in., for (lamina no., element no.) - (1,1)	(2,1)	(3,1)	(1,2)	(1,3)	(2,3)	(1,4)	(2,4)	(3,4)	Elements at max. strain	Is column at Euler load?	Elements at local buckling
1a	200	5.61	3.56	3.00	3.15	3.11	1.50	3.15	70	0.093	-----	-----	0.097	0.097	-----	0.093	-----	-----	---	Yes	1,2,4
1b	200	2.76	2.36	2.58	2.52	2.50	1.29	2.52	70	.079	-----	-----	.077	.090	-----	.079	-----	-----	---	Yes	1,2,4
1c	200	2.79	2.63	1.09	.96	.93	.54	.96	25	*.028	0.0	-----	.031	.036	-----	*.028	0.0	-----	---	Yes	1,2,4
1c	200	2.82	2.41	2.87	2.50	2.29	1.44	2.49	70	*.028	*.028	-----	*.077	*.126	-----	*.028	*.028	-----	---	Yes	1,2,4
1c	1000	7.01	4.73	2.86	4.00	2.67	1.45	4.00	70	*.028	.064	-----	.172	.226	-----	*.028	.064	-----	1,4	No	2
1e	200	3.83	2.15	1.41	2.19	.61	2.23	2.15	70	*.028	.049	-----	.052	.052	0.369	*.028	.049	-----	---	Yes	2,4
2a	200	6.22	3.22	1.68	1.99	1.23	1.99	1.98	50	.059	-----	-----	.059	.247	-----	.117	-----	-----	---	Yes	2,4
2b	200	3.00	2.17	1.66	1.66	1.73	1.38	1.66	50	.048	-----	-----	.048	.098	-----	.097	-----	-----	---	Yes	1,2
2c	200	5.05	2.00	1.11	1.46	.56	2.12	1.43	50	.034	-----	-----	.034	.034	.350	.062	.034	-----	---	Yes	1,2
3a	200	3.55	6.09	5.20	4.25	4.08	7.12	4.22	70	.316	.016	-----	.172	.172	-----	.316	.016	-----	---	Yes	2,4
3b	200	1.96	3.84	4.14	3.44	3.40	5.20	3.42	70	.175	*.014	0.0	.133	.159	-----	.175	*.014	0.0	---	Yes	2,4
3b	1000	7.09	4.71	4.28	5.10	4.16	2.28	5.10	70	.057	*.014	.032	.229	.309	-----	.057	*.014	.032	1,4	No	4
3c	200	2.62	4.64	3.30	3.36	1.92	7.47	3.29	70	.296	*.014	.005	.119	.119	.195	.296	*.014	.005	1,4	Yes	2,4
4a	200	4.63	4.32	5.93	3.65	4.05	2.02	3.52	70	-----	-----	-----	.124	.138	-----	.138	-----	-----	---	Yes	2,3,4
4b	200	2.34	2.79	4.72	2.73	3.74	1.87	2.68	70	-----	-----	-----	.090	.124	-----	.124	-----	-----	---	Yes	2,3,4

*This dimension was part of optimization-procedure input data.

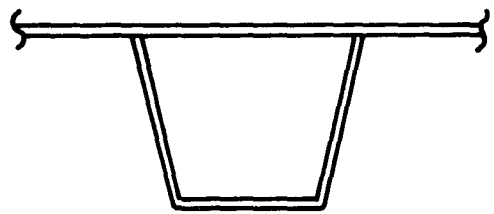

Configuration 1

Hat-stiffened panel

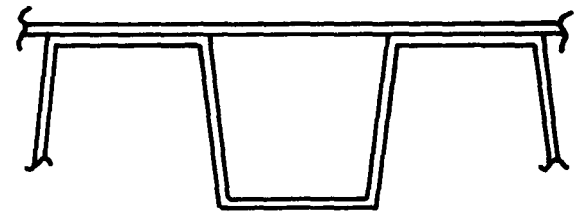

Configuration 2

Corrugation-stiffened panel

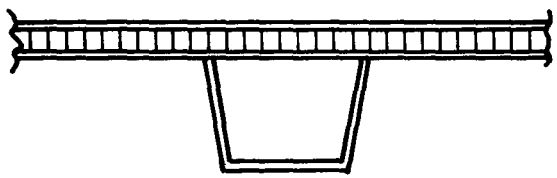

Configuration 3

Hat-stiffened honeycomb-core sandwich panel

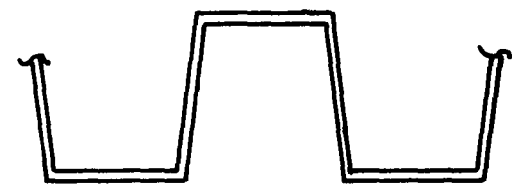

Configuration 4

Open-section corrugation panel

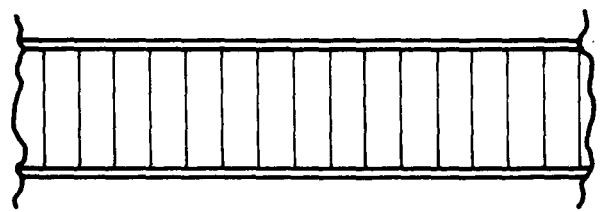

Configuration 5

Honeycomb-core sandwich panel

Figure 1.- Compression-panel configurations examined during the present study.

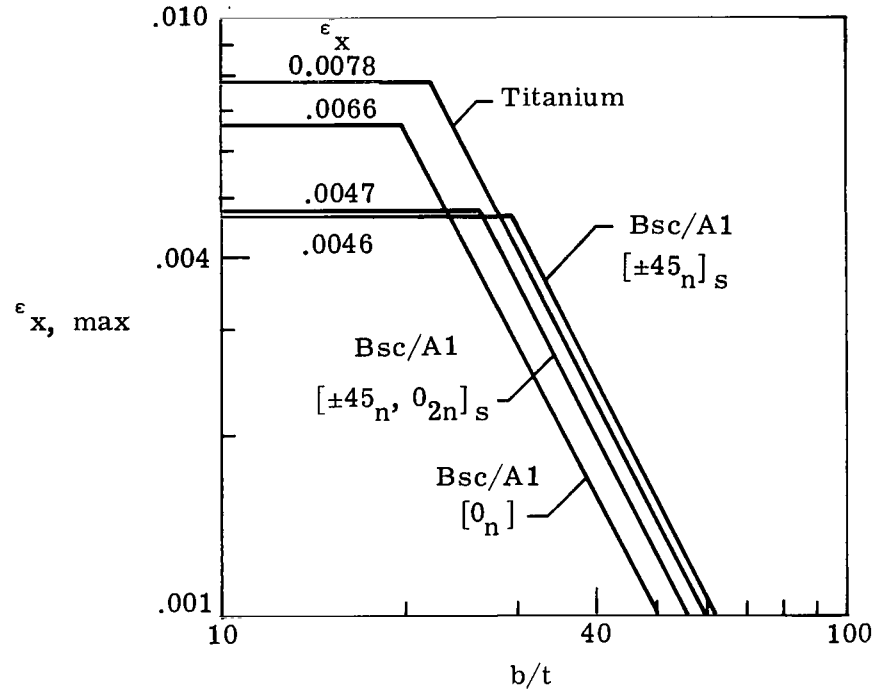

(a) Typical design curves used as local buckling constraints in optimization analysis.

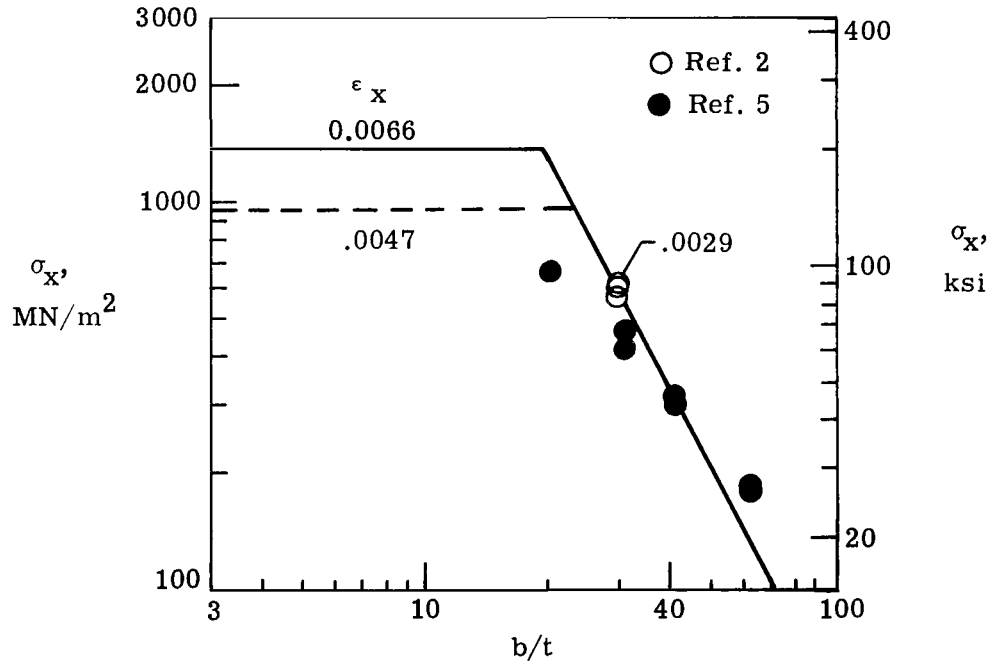

(b) Comparisons of 0° Bsc/Al design curves with experimental data.

Figure 2.- Strength and buckling curves for simply supported plate elements.

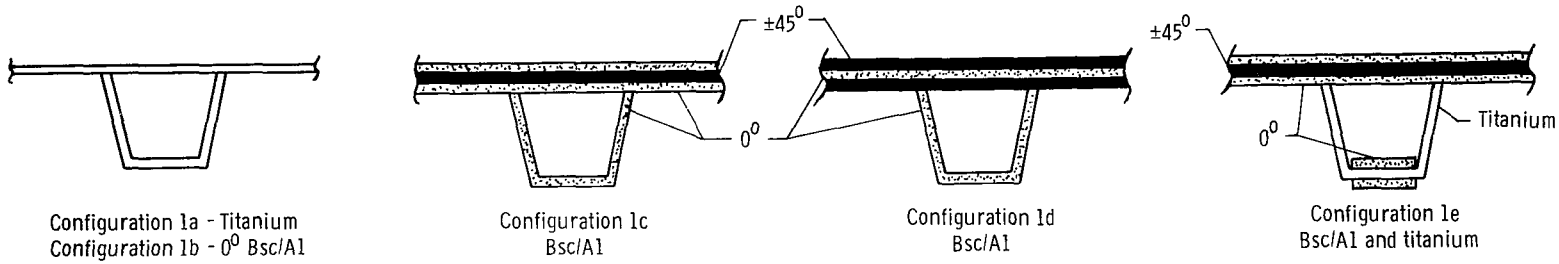

(a) Material distribution.

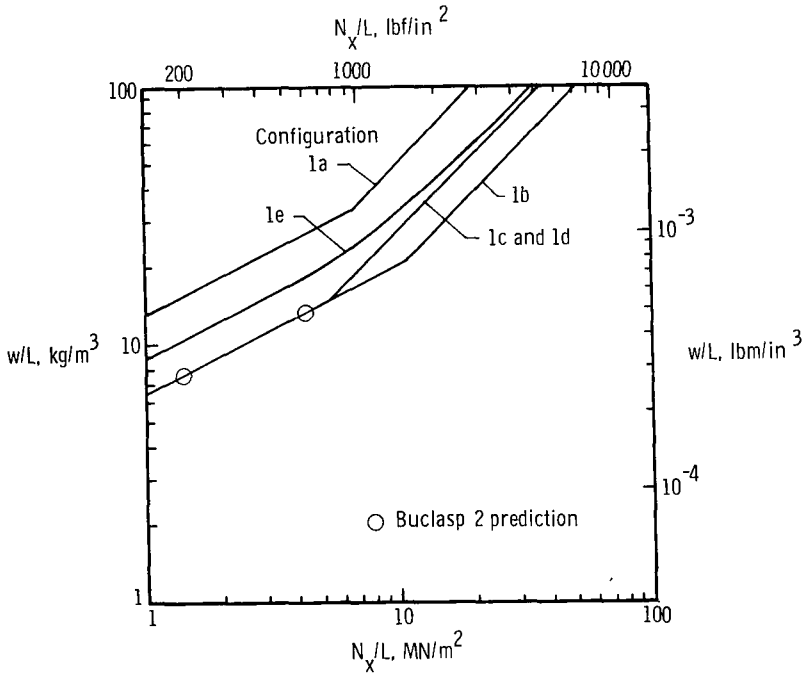

(b) Mass-strength curves.

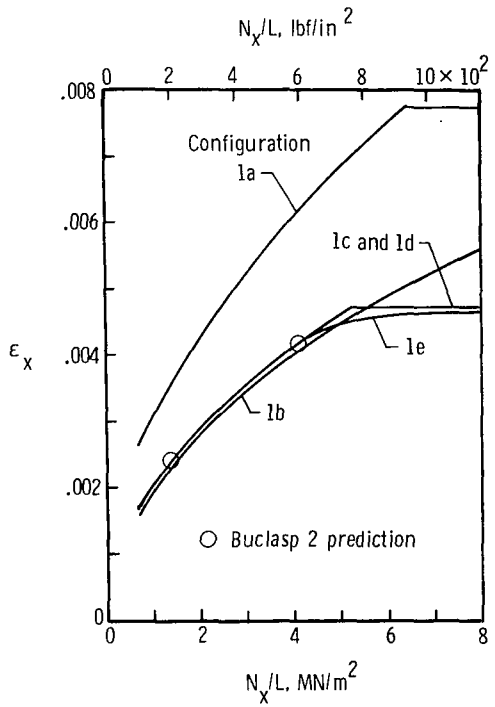

(c) Compressive strain-strength curves.

Figure 3.- Results of hat-stiffened panel analyses (configuration 1).

(a) Material distribution.

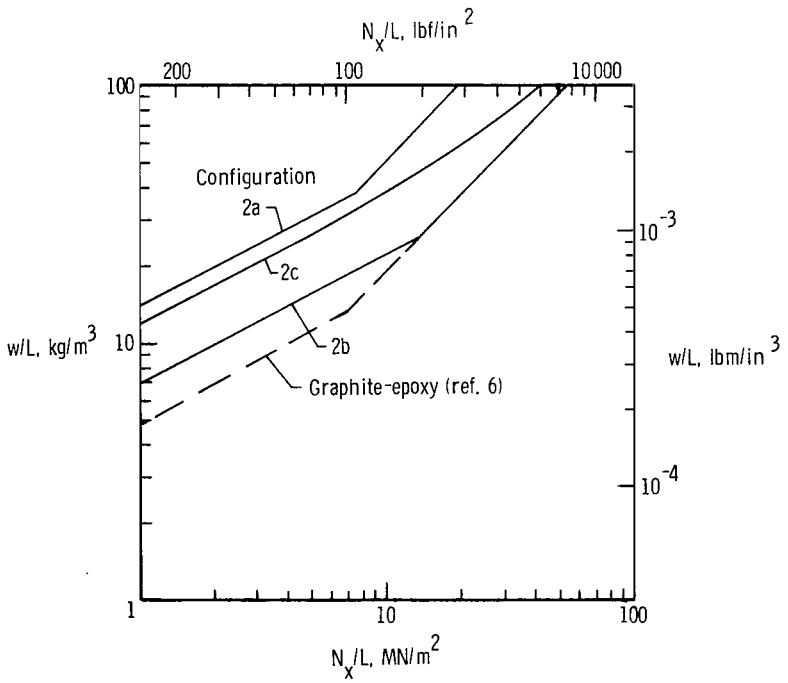

(b) Mass-strength curves.

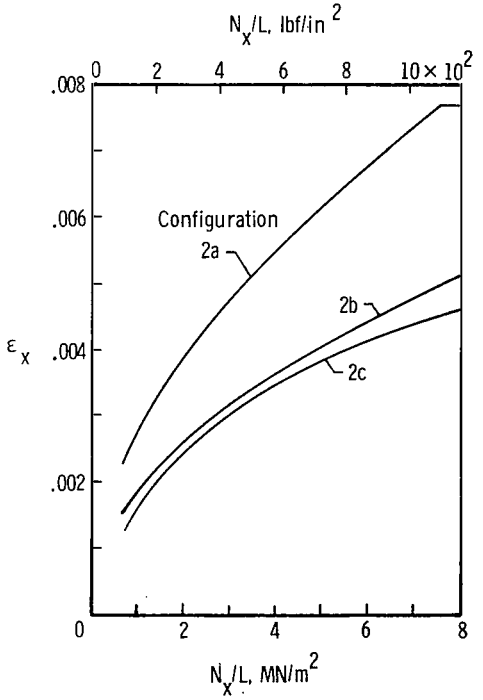

(c) Compressive strain-strength curves.

Figure 4.- Results of corrugation-stiffened panel analyses (configuration 2).

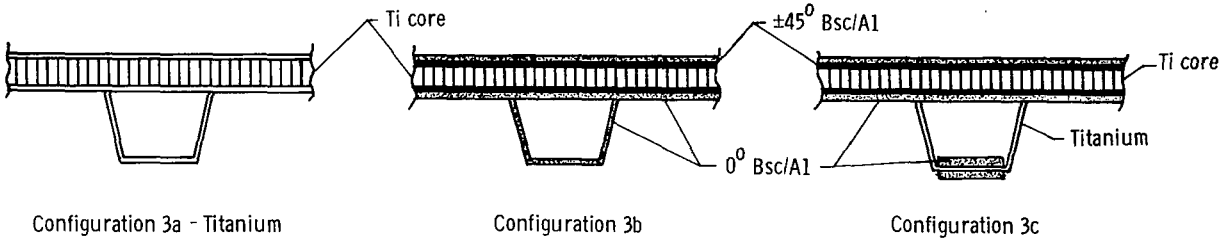

(a) Material distribution.

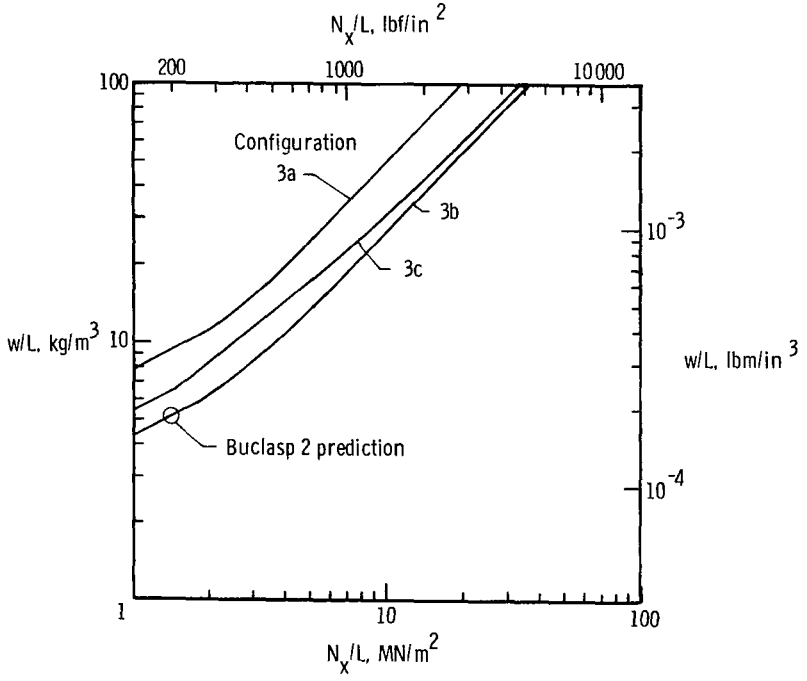

(b) Mass-strength curves.

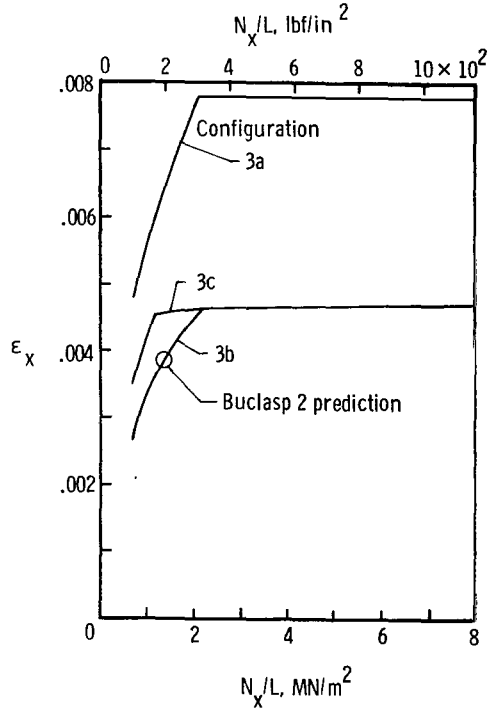

(c) Compressive strain-strength curves.

Figure 5.- Results of hat-stiffened honeycomb-core sandwich panel analyses (configuration 3).

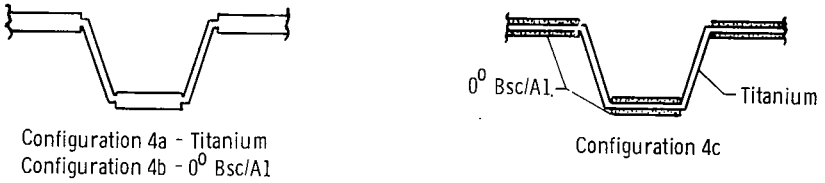

(a) Material distribution.

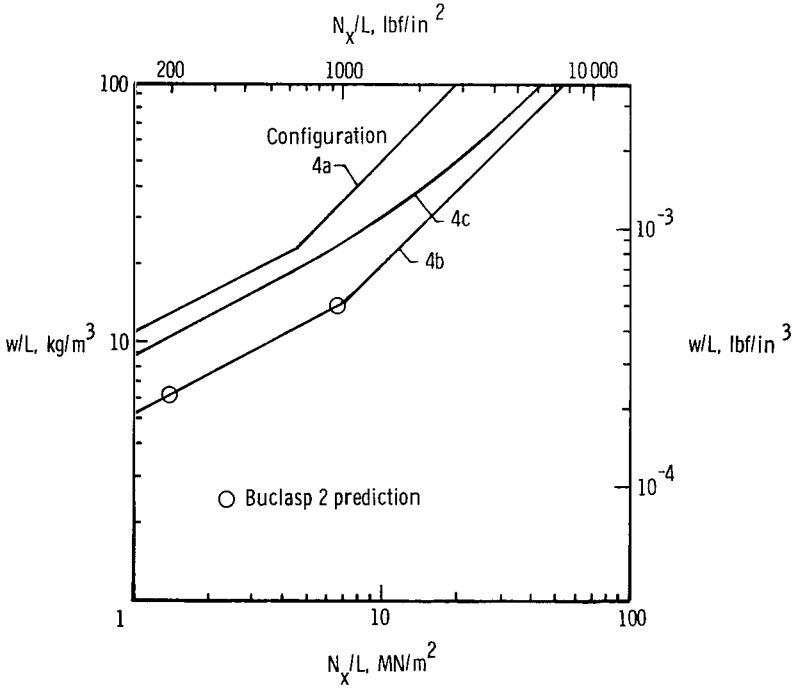

(b) Mass-strength curves.

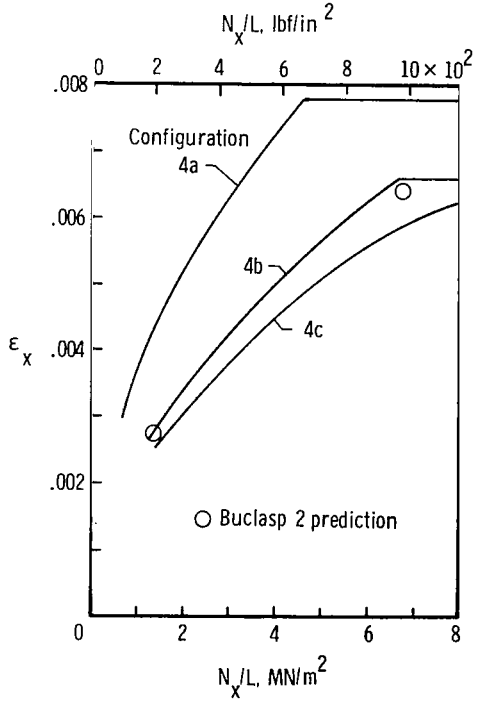

(c) Compressive strain-strength curves.

Figure 6.- Results of open-section corrugation panel analyses (configuration 4).

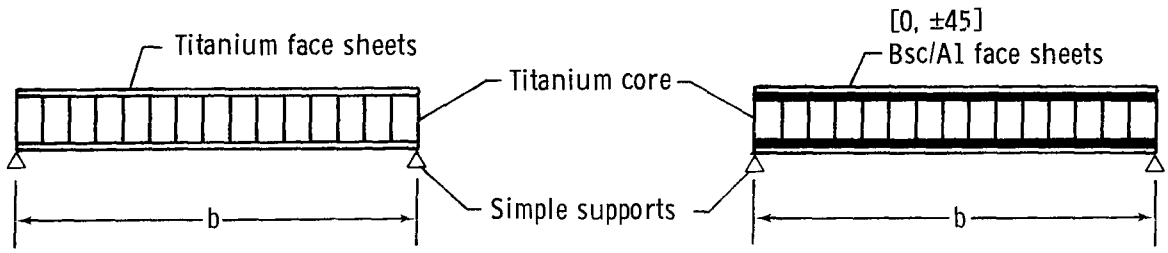

Configuration 5a ρ_{core} = 80 kg/m^3(5 lbm/ft^3)
Configuration 5b ρ_{core} = 160 kg/m^3(10 lbm/ft^3)
Configuration 5c ρ_{core} = 160 kg/m^3(10 lbm/ft^3)

(a) Material distribution.

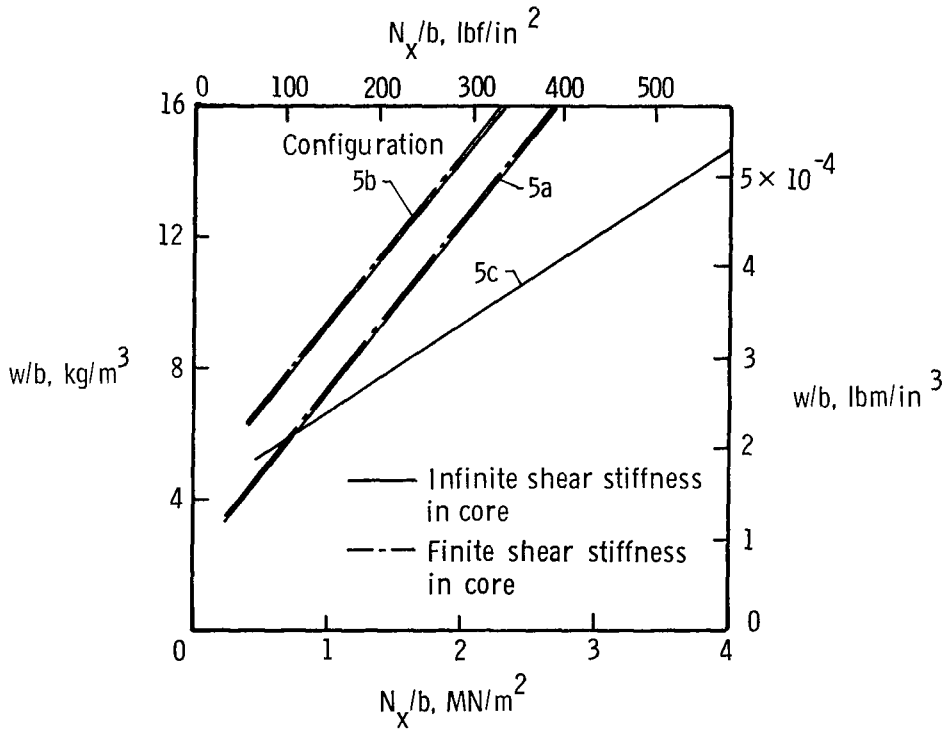

(b) Mass-strength curves.

Figure 7.- Results of honeycomb-core sandwich panel analyses (configuration 5).

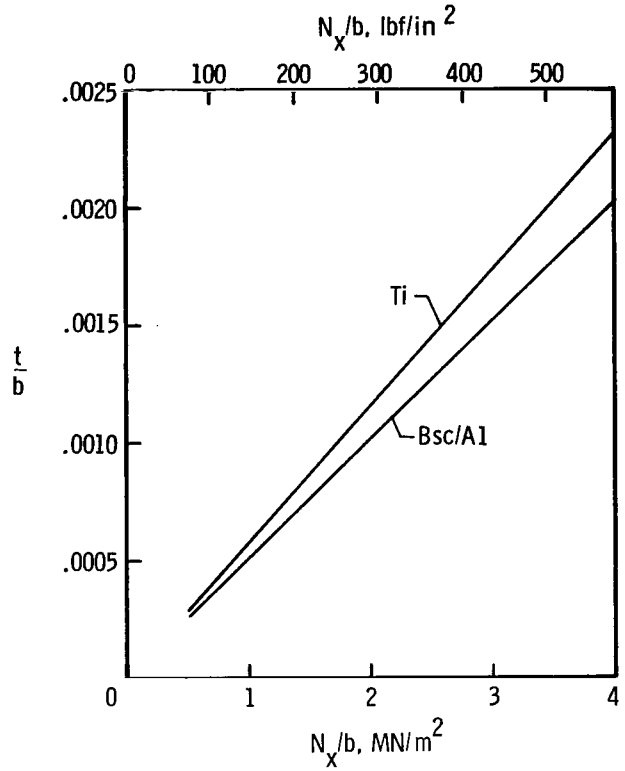

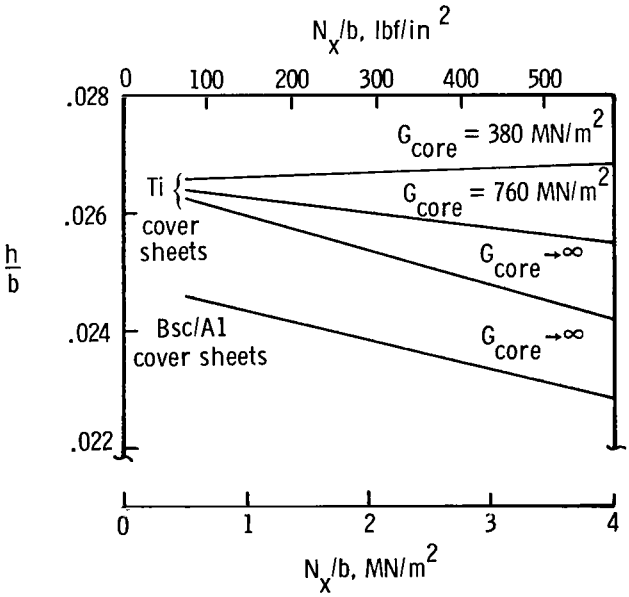

(c) Panel dimensions.

Figure 7.- Concluded.

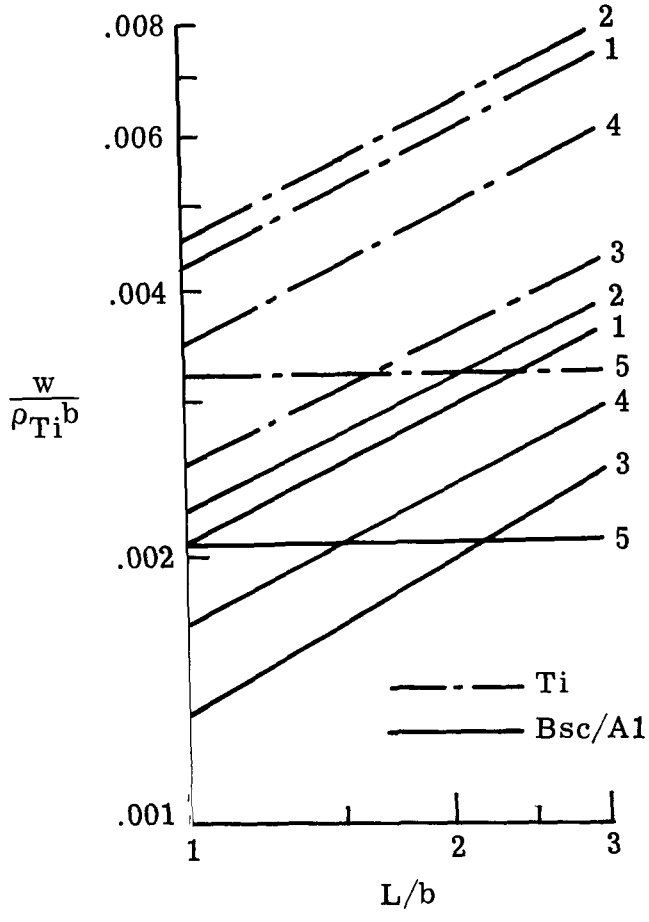

1 Hat-stiffened panel
2 Corrugation-stiffened panel
3 Hat-stiffened honeycomb-core sandwich panel
4 Open-section corrugation panel
5 Honeycomb-core sandwich panel

Figure 8.- Comparison of the structural efficiency of configurations 1 to 5 for N_x = 1.75 MN/m (10 000 lbf/in.) and b = 88.9 cm (35 in.).

Minimum gages		
Material	cm	in.
Ti	0.038	0.015
0^{o} Bsc/A1	.018	.007
$\pm 45^{o}$ Bsc/A1	.071	.028

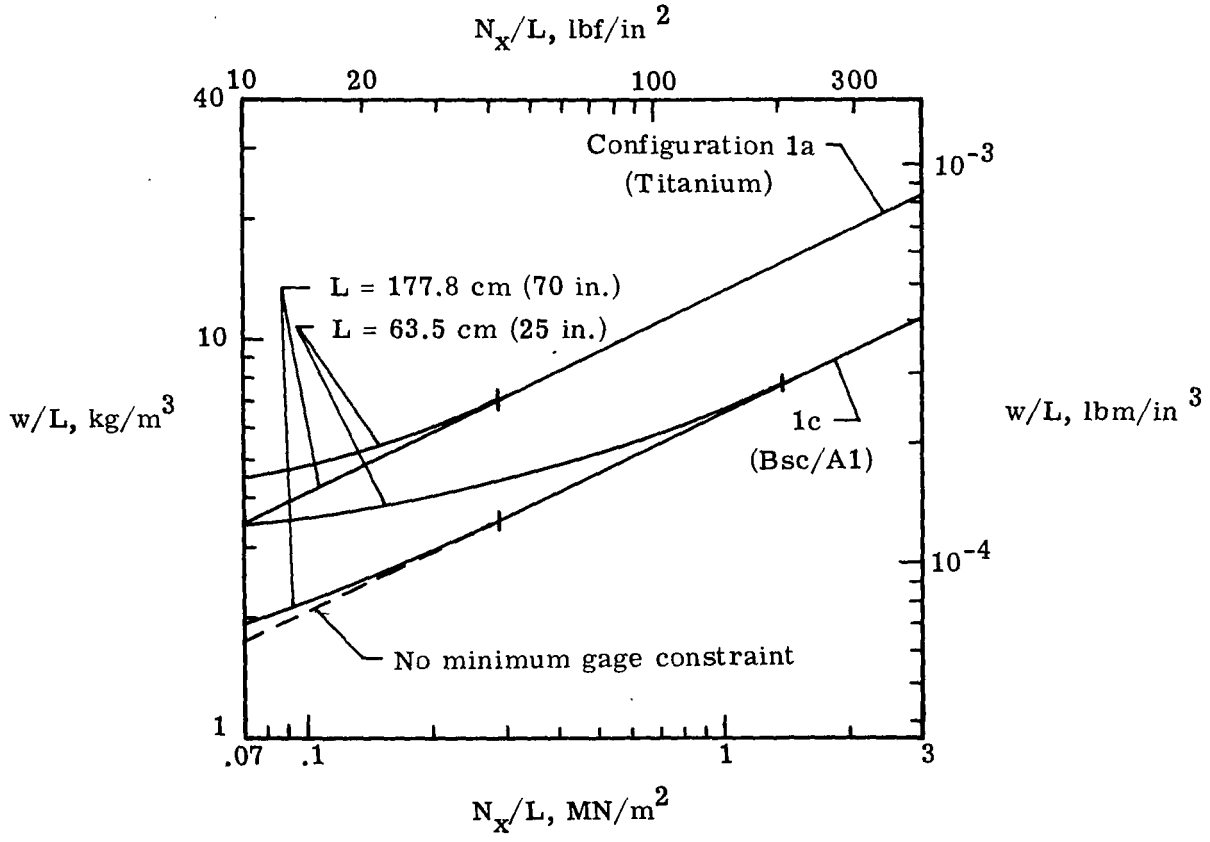

Figure 9.- Effect of minimum gage constraints on mass-strength curves for hat-stiffened panels (configuration 1).

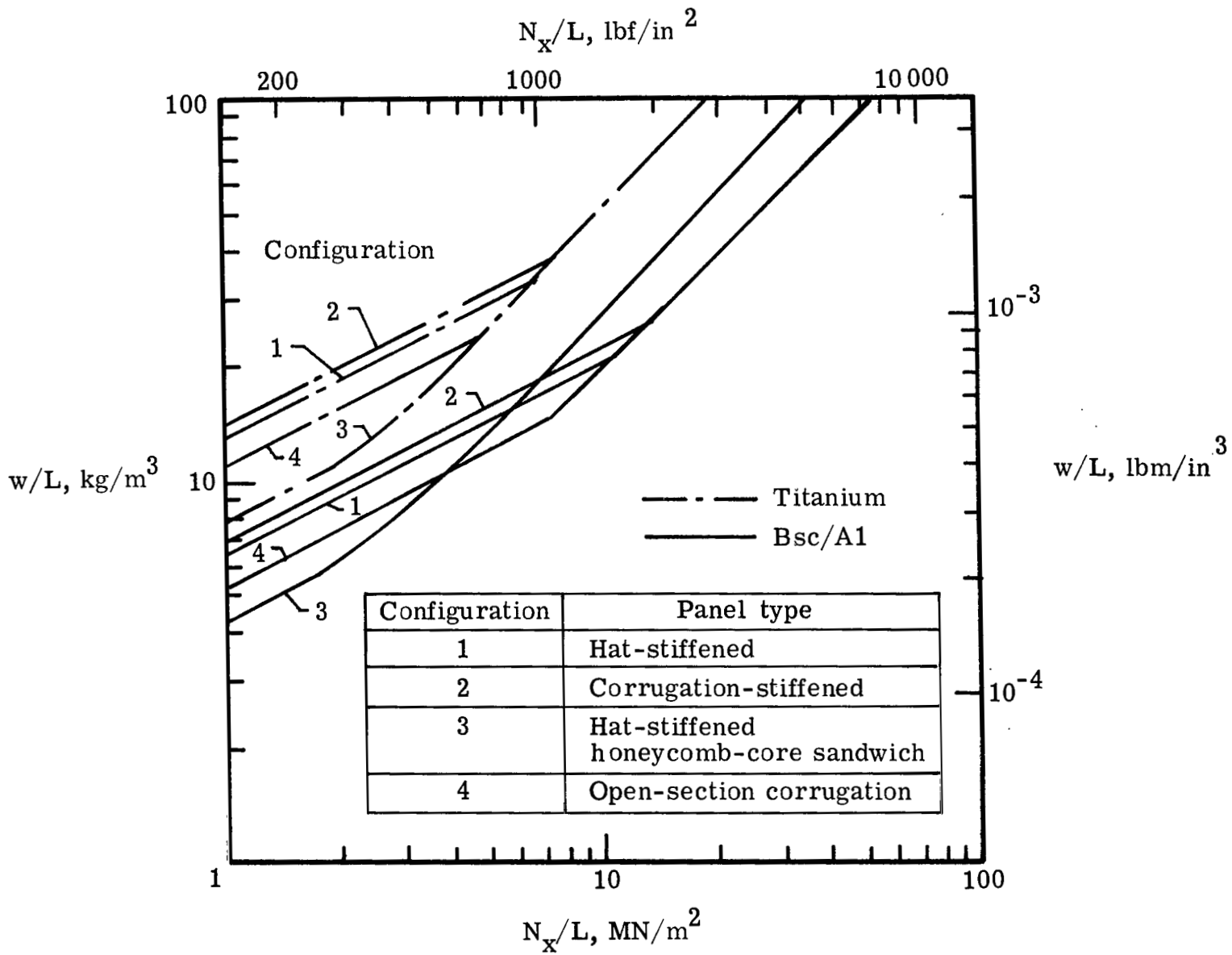

Figure 10.- Comparison of mass-strength curves for configurations 1 to 4.

NASA-Langley, 1976

"The aeronautical and space activities of the United States shall be conducted so as to contribute . . . to the expansion of human knowledge of phenomena in the atmosphere and space. The Administration shall provide for the widest practicable and appropriate dissemination of information concerning its activities and the results thereof."

—NATIONAL AERONAUTICS AND SPACE ACT OF 1958

NASA SCIENTIFIC AND TECHNICAL PUBLICATIONS

TECHNICAL REPORTS: Scientific and technical information considered important, complete, and a lasting contribution to existing knowledge.

TECHNICAL NOTES: Information less broad in scope but nevertheless of importance as a contribution to existing knowledge.

TECHNICAL MEMORANDUMS: Information receiving limited distribution because of preliminary data, security classification, or other reasons. Also includes conference proceedings with either limited or unlimited distribution.

CONTRACTOR REPORTS: Scientific and technical information generated under a NASA contract or grant and considered an important contribution to existing knowledge.

TECHNICAL TRANSLATIONS: Information published in a foreign language considered to merit NASA distribution in English.

SPECIAL PUBLICATIONS: Information derived from or of value to NASA activities. Publications include final reports of major projects, monographs, data compilations, handbooks, sourcebooks, and special bibliographies.

TECHNOLOGY UTILIZATION PUBLICATIONS: Information on technology used by NASA that may be of particular interest in commercial and other non-aerospace applications. Publications include Tech Briefs, Technology Utilization Reports and Technology Surveys.

Details on the availability of these publications may be obtained from:

SCIENTIFIC AND TECHNICAL INFORMATION OFFICE

NATIONAL AERONAUTICS AND SPACE ADMINISTRATION

Washington, D.C. 20546